JOURNAL OF NEUROTRAUMA 31:803–818 (May 1, 2014)

DOI: 10.1089/neu.2013.3143

Astrocytic and Vascular Remodeling in the Injured Adult Rat Spinal Cord after Chondroitinase ABC Treatment

Ulla Milbreta,[1,2] Ysander von Boxberg,[1] Philippe Mailly,[3] Fatiha Nothias,[1] and Sylvia Soares[1]

Abstract

Upregulation of extracellular chondroitin sulfate proteoglycans (CSPG) is a primary cause for the failure of axons to regenerate after spinal cord injury (SCI), and the beneficial effect of their degradation by chondroitinase ABC (ChABC) is widely documented. Little is known, however, about the effect of ChABC treatment on astrogliosis and revascularization, two important factors influencing axon regrowth. This was investigated in the present study. Immediately after a spinal cord hemisection at thoracic level 8–9, we injected ChABC intrathecally at the sacral level, repeated three times until 10 days post-injury. Our results show an effective cleavage of CSPG glycosaminoglycan chains and stimulation of axonal remodeling within the injury site, accompanied by an extended period of astrocyte remodeling (up to 4 weeks). Interestingly, ChABC treatment favored an orientation of astrocytic processes directed toward the injury, in close association with axons at the lesion entry zone, suggesting a correlation between axon and astrocyte remodeling. Further, during the first weeks post-injury, ChABC treatment affected the morphology of laminin-positive blood vessel basement membranes and vessel-independent laminin deposits: hypertrophied blood vessels with detached or duplicated basement membrane were more numerous than in lesioned untreated animals. In contrast, at later time points, laminin expression increased and became more directly associated with newly formed blood vessels, the size of which tended to be closer to that found in intact tissue. Our data reinforce the idea that ChABC injection in combination with other synergistic treatments is a promising therapeutic strategy for SCI repair.

Key words: axon remodeling; blood–brain barrier; glial scar; laminin; neoangiogenesis

Introduction

Functional recovery from spinal cord injury (SCI) is largely impeded by the glial scar, formed by reactive astrocytes that within hours after the lesion start to surround the injury site, where they create a physical and molecular barrier for axonal regeneration. Thus, high concentrations of axon growth-inhibitory chondroitin sulfate proteoglycans (CSPG), mainly produced by reactive astrocytes, are found in the scar tissue, which is at the same time characterized by breakdown of the blood–brain barrier (BBB).[1–5] CSPG, as well as heparan sulfate proteoglycans (HSPG), are also found in the basement membrane (BM) of blood vessels.[6,7] Moreover, secondary injuries and chronic functional deficits after SCI are associated with alterations of the microvasculature,[8] including increased BBB permeability,[9] modified vascular morphology,[10–12] and BM duplication.[13,14]

Further, the giant protein AHNAK (700 kDa), expressed in an intact central nervous system (CNS) only by endothelial cells and pericytes, and specifically associated with tight junctions (TJ) of blood vessels belonging to the BBB,[15] is strongly expressed within the lesion site, both in blood vessels and in cells forming at later stages post-injury the inner border of cystic cavities, in front of the astrocytic scar.[12] Interestingly, after SCI, CSPG expression remains detectable at the interface of reactive astrocytes and AHNAK-positive cells even at long term.[12]

Degradation of CSPG through selective removal of glycosaminoglycan (GAG) side chains by the bacterial enzyme chondroitinase ABC (ChABC) renders the scar tissue less inhibitory for axon growth.[4,16,17] In different SCI models, a positive effect of ChABC treatment could be demonstrated,[18–23] such as improvement in forelimb performance in rats,[24,25] and recovery of specific locomotor skills in cats.[26] Combining ChABC treatment with peripheral nerve autograft resulted in extensive axon regeneration over rather long distances and greatly enhanced recovery of the functions of the affected forelimb[27] or the diaphragm.[28] More recently, combinatory treatment with anti-Nogo-A delivery and rehabilitation showed a functional recovery that was significantly better than any of the individual treatments alone.[29]

[1]Neuroscience Paris Seine/UMR8246/U1130/UMCR18, IBPS/UPMC Univ Paris 06, Paris, France.
[2]Nanyang Technological University, School of Chemical and Biomedical Engineering, Singapore.
[3]CIRB, UMR7241, U1050, Collège de France, Paris, France.

While the beneficial effect on axonal plasticity after SCI is widely documented, little was known so far about how ChABC treatment may affect glial scar structure and revascularization of the lesioned tissue, two factors having a major impact on the regenerative capacity of traumatic adult spinal cord. These issues were the subject of the present study. Thus, we demonstrate for the first time that ChABC treatment reduces not only the chemical but also the physical barrier to axon remodeling, while at the same time increasing astrocyte dynamics and remodeling and rendering the process of revascularization of the lesion site more efficient at long term.

Methods

All experimental procedures on animals were in accordance with European Community directives (86/609/EEC; authorization number 91-78 to F. Nothias).

Spinal cord injury and drug delivery

Fifty adult female (200–250g) Wistar rats (Janvier, Berthevin, France) were anesthetized with intraperitoneal injection (2.25 mL/kg) of a solution containing xylazine (5 mg/kg; Rompun 2%, Bayer, Puteaux, France) and ketamine (50 mg/kg; Imalgène 1000, Rhône Merieux, France). After laminectomy of thoracic T8-9 vertebrae, the right side of the spinal cord was entirely transected using microscissors.[12,30] Immediately after the injury, half of the lesioned animals received intrathecal injections at the sacral level of protease-free ChABC (Seikagaku, Japan) or control enzyme penicillinase (P-ase; Sigma-Aldrich), and then every third day for a total of four injections (days 0, 3, 6, 9) using a 0.5 mL Hamilton syringe (VWR, France). Each animal was injected 3 μL of ChABC (0.15 units per dose) in 27 μL of artificial cerebrospinal fluid (CSF; Harvard Apparatus) or 14 μL of P-ase (30 μg/mL) in 16 μL of CSF, as described previously.[18,20]

We chose to use intrathecal injection of ChABC to avoid secondary injuries that would have been generated by reopening the injured animals for consecutive injections. This mode of administration had been widely used for drug delivery in experimental models.[31] The observed decrease in CSPG immunolabeling intensity at the lesion site (Fig. 1), as well as the enhanced axonal regeneration (Fig. 2,3,4,5B), proved that the efficacy of our administration mode was comparable to previously used methods of ChABC injection.

Immunohistochemistry

After survival times of 1, 2, 4, and 10 weeks post-injury, animals were deeply anesthetized with an intraperitoneal injection of sodium pentobarbital (100 mg/kg) and transcardially perfused with saline followed by 400 mL of 4% paraformaldehyde (PFA) in phosphate buffer. Spinal cords were removed and postfixed for 2 h in the same solution followed by cryoprotection in 30% sucrose at 4°C for 48 h, embedded in Tissue Freezing Medium (Leica; France), and cut into 30 μm thick horizontal sections. Sections were permeabilized with 0.3% Triton X-100 in phosphate buffered saline (PBS, pH 7.4), and nonspecific binding sites were blocked with 10% normal goat serum (NGS) in PBS for 1 h.

Slides were incubated overnight at room temperature with the following antibodies: monoclonal mouse anti-CSPG chondroitin sulfate antibody (CS-56) (Sigma-Aldrich; 1:200), recognizing the GAG portion of CSPG; rabbit anti-glial fibrillary acidic protein (GFAP) (Dako; 1:2000); rabbit anti-laminin (Sigma-Aldrich; 1:100) to identify blood vessel basement membranes, rabbit anti-

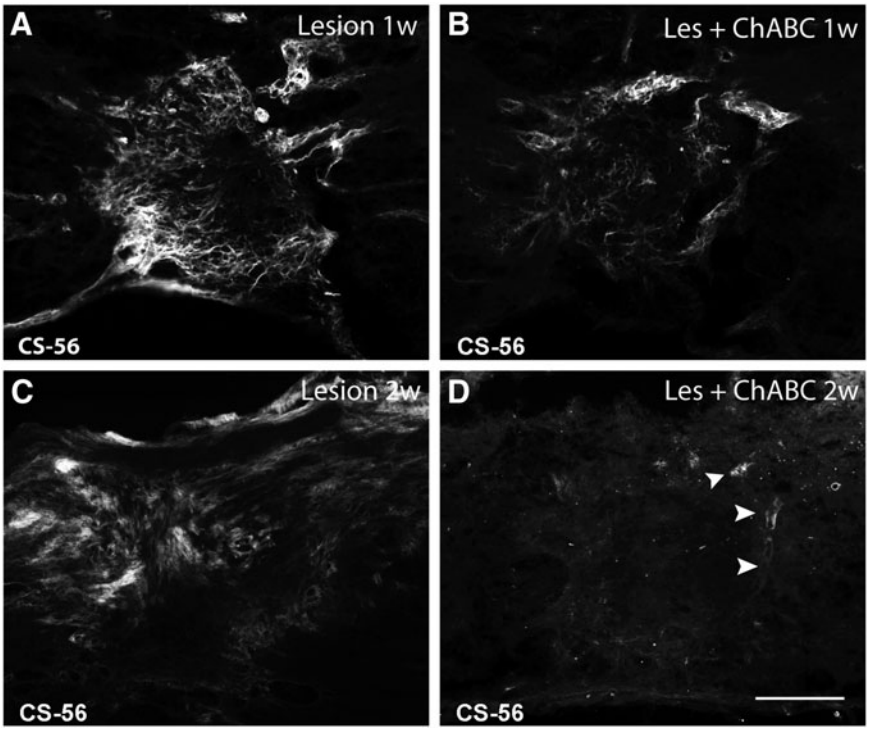

FIG. 1. Efficient cleavage of chondroitin sulfate proteoglycans (CSPG) glycosaminoglycan side chains in a thoracic spinal cord hemisection lesion by intrathecal injections of chondroitinase ABC (ChABC) at the sacral level. CSPG (CS-56) immunofluorescence on spinal cord horizontal sections after 1 (**A**, **B**), and 2 weeks (w) (**C**,**D**) post-injury, in untreated (Lesion), and ChABC-treated (Les+ChABC) animals. In contrast to the persistent, strong CSPG labeling observed in untreated animals (A,C), after ChABC treatment (B,D) only traces of immunolabeling are left at the borders of the injury, particularly on blood vessels (arrowheads in D). Bar, 200 μm.

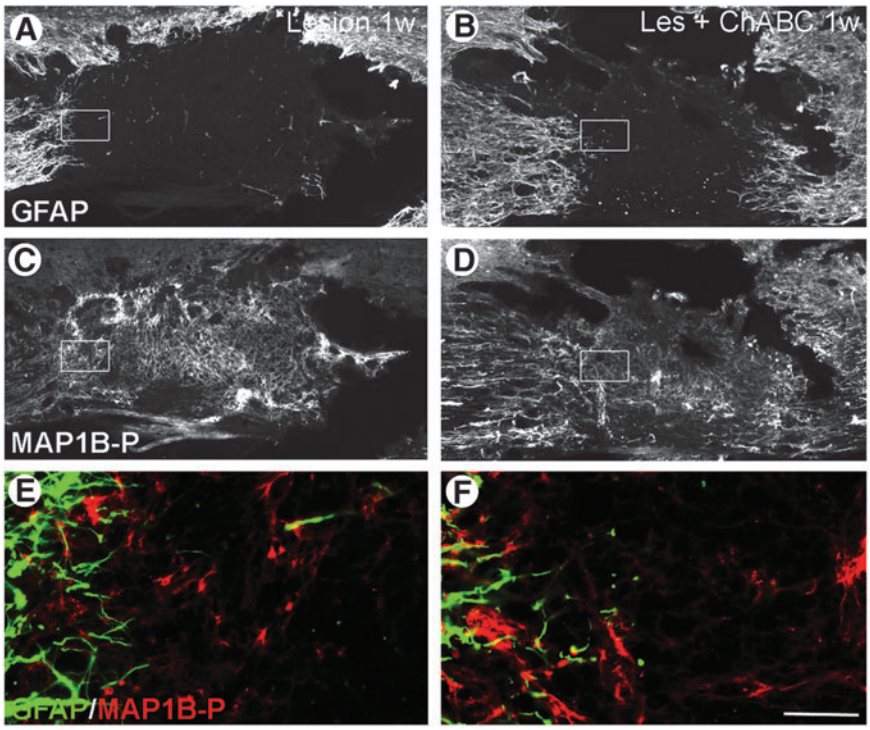

FIG. 2. Glial scar evolution and axon remodeling 1 week post-injury, with or without chondroitinase ABC (ChABC) treatment; double immunofluorescence labeling for glial fibrillary acidic protein (GFAP) (**A,B, E, F**; green on merge image), and phosphorylated microtubule associated protein 1B (MAP1B-P) (**C, D, E, F**; red on merge image) on spinal cord sections of untreated (Lesion) and ChABC-treated (Les + ChABC) animals. E and F are higher magnification merge images of insets in A,C and B,D, respectively. GFAP labeling is less intense after the treatment (compare A and B), and astrocytic extensions are longer and more often oriented toward the injury site. Bar: A–D, 130 μm; E-F, 15 μm. Color image is available online at www.liebertpub.com/neu

AHNAK (clone 5; homemade; 1:5[12] to label blood–brain barrier-forming vessels, and non-neuronal cells that invade the injury site ; monoclonal mouse anti-phosphorylated isoform of MAP1B-P (1:150); hybridoma generously provided by Dr I. Fischer[32] to detect axons undergoing remodeling[30,33]; monoclonal anti- rat endothelial cell antigen (RECA-1) (Abcam; 1:25) to identify endothelial cells; monoclonal SMI 71 (Covance; 1:100) to identify rat blood-brain barrier-forming endothelial cells; monoclonal ZO-1 (Invitrogen; 1:1000) labeling tight junctions. Slides were subsequently washed with 5% NGS in PBS and incubated with appropriate Alexa-coupled secondary antibodies (Invitrogen) in a light-protected tray on a shaker for 2 h at room temperature. Sections were slide-mounted and coverslipped with Mowiol.

Analysis and photographic documentation (in particular for composite reconstruction) were performed on an Apotome-equipped Zeiss Axiovert 200 inverted microscope, and confocal images were obtained using a Leica DMI 6000B laser scanning microscope. Particular care was taken to always compare sections representing the same levels inside the injury for treated and untreated animals.

SDS PAGE and Western blotting

Animals were deeply anesthetized with sodium pentobarbital (100 mg/kg), and transcardially perfused with saline. Six small spinal segments (the lesion site itself, 1 cm rostral, 1 cm caudal to the lesion; the same three from the contralateral side) were collected at 1, 2, and 4 weeks post-injury, frozen and stored at − 80°C. Spinal segments were homogenized in lysis buffer (62.5 mM Tris-HCl, pH 6.8, 4 M urea, 1% NP-40, 0.5% Triton X-100, 0.5 mM orthovanadate, 1 mM PMSF, 1 mM benzamidine, 2 mM EDTA, 2 mM EGTA, and 10% protease inhibitor cocktail; Sigma), and samples were centrifuged for 5 min at 10,000*g*. Protein content was measured using the standard Bradford Assay.

Sodium dodecyl sulfate polyacrylamide gel electrophoresis was performed on a microscale as previously described.[34] Acrylamide concentration for resolution of AHNAK bands was 7.5%, and gels were run until the front of migration had left the gel; for other proteins (e.g., actin for reference) acrylamide concentration was 9%. After transfer onto nitrocellulose, membranes were blocked in 5% nonfat dry milk in PBS, incubated with primary antibodies for AHNAK (antiserum against clone A5 fusion protein, 1:1000[12]), and beta-actin (C4, Santa Cruz, 1:500) in 1% nonfat dry milk and 0.05% Tween-80 in PBS, followed by appropriate secondary antibodies coupled to alkaline phosphatase (Jackson ImmunoResearch, Beckman-Coulter, Villepinte, France), and revelation with the NBT/BCIP reagent.

Quantitative analyses

Measurement of GFAP/MAP1B-P positive areas. Using confocal microscope images of sections representing the lesion sites of nine treated and nine untreated animals, we determined the relation between total primary injury area delimited by GFAP-positive astrocytes (glial scar, dark grey circle in Fig. 5A), and the relative areas contained therein that were covered by astrocytic processes, or MAP1B-P-positive axons. Lesions from 1 to 4 weeks post-injury (three animals/time post-injury/experimental condition) were evaluated on three sections/animal. Using Fiji software,[35] after defining minimum and maximum thresholds, local pixel intensities corresponding to GFAP and MAP1B-P fluorescent channels were segmented, and corresponding areas calculated. Statistical correlations between labeling, treatment, and age were quantified using the Student *t* test (StatView software).

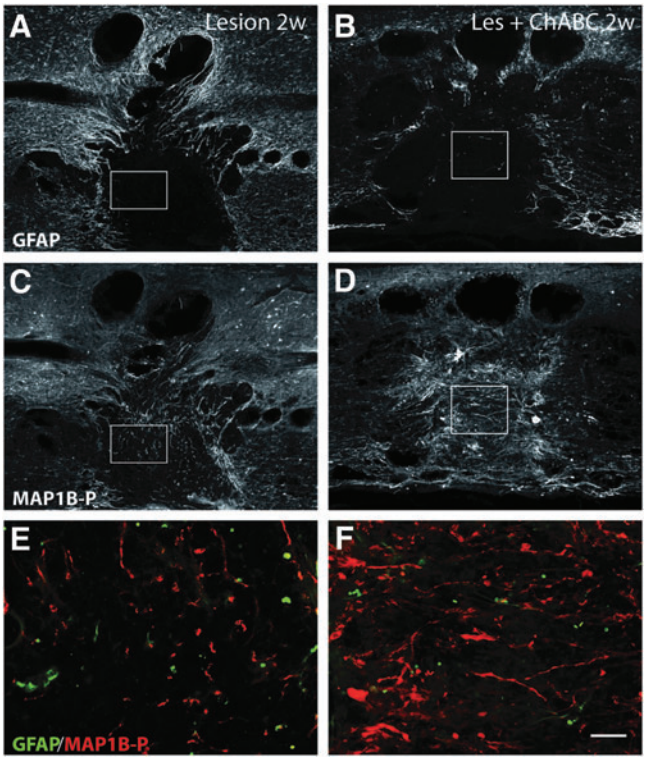

FIG. 3. Glial scar evolution and axon remodeling 2 weeks post-injury; double immunofluorescence labeling for glial fibrillary acidic protein (GFAP) (**A,B, E, F**; green on merge image) and phosphorylated microtubule associated protein 1B (MAP1B-P) (**C, D, E-F**; red on merge image) on spinal cord sections of untreated, and chondroitinase ABC (ChABC)-treated animals. E and F are higher magnification merge images of insets in A,C and B,D, respectively). Note that ChABC treatment renders the glial scar less dense (compare A with B), and considerably increases the total number of axons in the injury site, as well as the percentage of axons properly oriented in the rostrocaudal direction (compare C with D). Bar: A-F, 130 μm; G,H, 25 μm. Color image is available online at www.liebertpub.com/neu

Directionality analysis. Preferred orientation, or directionality, of GFAP-positive astrocytic processes and MAP1B-P-positive axons was measured using images from the primary injury site and cavity borders (three sections/animal; three animals/age/experimental condition) taken on an Apotome Axiovert 200 inverted microscope equipped with an AxioCamera (Zeiss) and $\times$20 objective. Directionality analysis was performed using Fiji software with the directionality plugin (ImageJ, NIH), according to user guidelines (see tutorial by J.-Y. Tinevez, http://fiji.sc/wiki/index.php/Directionality). Briefly, the orientation of all astrocytic and axonal processes within each analyzed picture was expressed as the angle formed against the horizontal axis of the image, defined as 0 degrees and chosen as arbitrary reference (see Fig. 5C). For each image, the total number of processes growing into a given direction (angle) was then calculated and presented as a Gaussian function in a histogram showing the distribution frequencies for the different angles. Finally, separately for each image, preferred directionalities were compared between GFAP-positive astrocytic processes and MAP1B-P-positive axons and the results (i.e., the degree of coincidence between the orientations of axons and astrocyte processes) statistically analyzed for treated versus untreated animals at different time points post-injury using a two-tailed unpaired *t* test (StatView software). Representative confocal microscope images are also shown (Fig 5C).

Quantitative evaluation of Western blots. For quantitative evaluation of AHNAK, Western blot membranes were scanned, and image analysis was performed using Fiji software with a gel analysis plugin (ImageJ, NIH) according to user guidelines. Briefly, a rectangle was drawn around the protein band with maximum extent/intensity, and the same size rectangle was applied to all other bands of interest (see tutorial by L.P. Miller http://lukemiller.org/index.php/2010/11/analyzing-gels-and-western-blots-with-image-j/). Three independent experiments were quantified, and results were statistically compared using *t* test (GraphPadPrism software).

Morphometric analysis of laminin-positive tubular structures. Confocal immunofluorescence images were captured using an inverted Leica DMI 6000B laser scanning microscope (zoom $\times$40). At least three animals per condition were analyzed, and three images from every injury site were collected. Laminin-positive tubular structures that were also positive for RECA-1 and had a luminal diameter of more than 5 μm were counted and classified in a diameter distribution chart, divided into four subgroups (5–8 μm; 8–15 μm; 15–30 μm, and 30–90 μm). After statistical evaluation (two-tailed unpaired *t* test, StatView software), results were finally compared with the morphometric blood vessel analysis of Ormandzhieva.[36]

Results

Intrathecal ChABC injections induce CSPG degradation at the lesion site

Consistent with earlier studies on SCI reporting increased CSPG production at the injury site,[4,37–41] Fig. 1A shows important CSPG immunoreactivity (IR) boarding the lesion center at 1 week post-injury, becoming maximal at 2 weeks post-injury (Fig. 1C), before decreasing to almost undetectable levels by 4 weeks post-injury (not shown; note that CSPG labeling is almost undetectable in control tissue). CSPG labeling was found on reactive astrocytes, blood vessels,[42,43] and thin strands resembling extracellular matrix (ECM) deposits. ChABC treatment greatly diminished CSPG IR at all time points analyzed. Occasionally, some traces of CSPG were still found in the lesion site (Fig. 1B,D), essentially on blood vessels (Fig. 1D, arrowheads). These results show that repeated intrathecal injections at the sacral level of ChABC efficiently cleave CSPG GAG side chains at the thoracic injury site, in spite of the great distance (about 9 cm) between lesion and injection sites.

ChABC treatment modifies astrocyte rearrangement and scar formation, associated to axon remodeling through the lesion site

In addition to its well documented effect on axonal remodeling, we show here that ChABC treatment had a remarkable effect on astrogliosis and, hence, glial scar evolution that was examined using GFAP labeling. In addition, our double immunolabeling analysis at various times post-injury provided evidence that astrocyte processes and axons colocalized more frequently, exhibiting similar orientations at the entry zone of the lesion site, suggesting that their remodeling may be correlated.

Astrocyte remodeling and scar formation. At 1 week post-injury in untreated and P-ase-treated animals, astrocytes underwent extensive astrogliosis, with their processes becoming hypertrophic, and GFAP IR around the injury site strongly increasing. Numerous astrocytic extensions were oriented toward the injury site (Fig. 2A), similar to what was recently shown in a mouse spinal cord injury model.[44] Other GFAP-positive astrocytes started to create a dense web of interdigitated processes walling off the cavity, first signs of

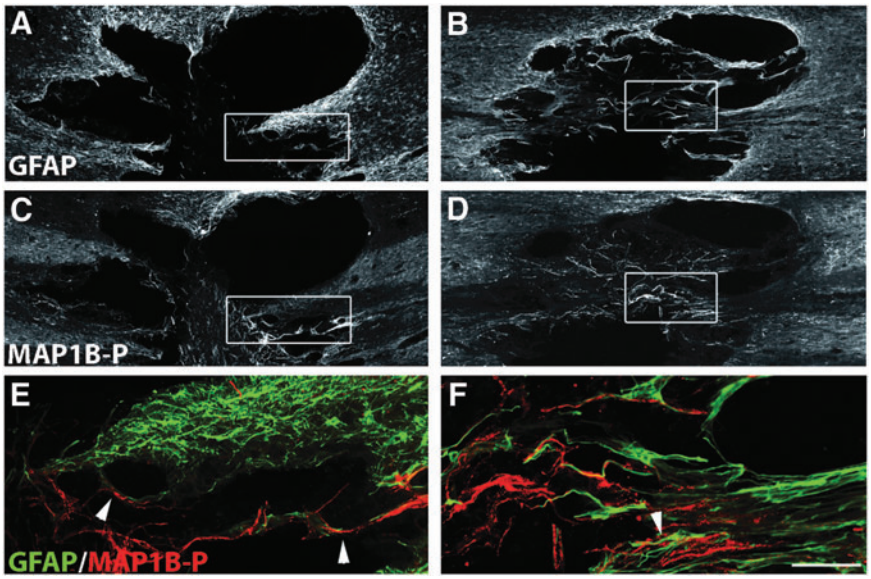

FIG. 4. Glial scar evolution and axon remodeling at 4 weeks post-injury; double immunofluorescence labeling for glial fibrillary acidic protein (GFAP) (**A,B, E, F;** green in merge image) and phosphorylated microtubule associated protein 1B (MAP1B-P) (**C, D, E, F;** red in merge image) on spinal cord sections of untreated (**A,C,E**), and chondroitinase ABC (ChABC)-treated animals (**B,D,F**). E and F are higher magnification merge images of insets in A,C, and B,D, respectively. Note that after treatment with ChABC, the GFAP-positive scar is not completely developed even at long term. Numerous axons are found in the injury site, oriented in the same direction as the astrocytic extensions (arrowhead, F), a phenomenon also observed in untreated animals, albeit much less frequently (arrowheads in E). Bars: A-D, 240 μm; E,F, 65 μm. Color image is available online at www.liebertpub.com/neu

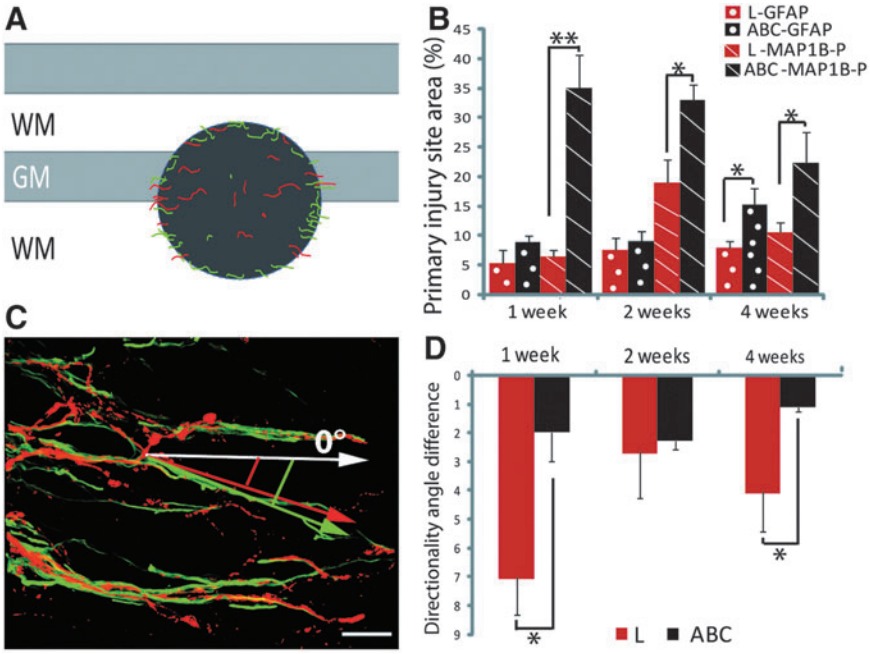

FIG. 5. Quantification of number and orientation of astrocytic processes and phosphorylated microtubule associated protein 1B (MAP1B-P) positive axons in untreated (red bars), and chondroitinase ABC (ChABC)-treated (black bars) animals. (**A**) Schematic representation of a horizontal section of the spinal cord. The dark grey area depicts the primary injury site delimited by the outer border of the glial scar, where densities of astrocytic processes (green) and axons (red) were measured. (**B**) Quantification of the area of the injury site occupied by glial fibrillary acidic protein (GFAP)- (dotted bars), and MAP1B-P-positive fibers (hatched bars) between 1 and 4 weeks post-injury. (**C**) Example of a three-dimensional reconstruction based on confocal images of the injury site from a ChABC-treated animal at 2 weeks post-injury, showing codistribution of MAP1B-P positive fibers (red) with GFAP-positive (green) processes. The directionality of GFAP-positive and MAP1B-P-positive structures is measured against the horizontal axis defined arbitrarily as angle 0 degrees, and differences between the angles of orientation of GFAP- and MAP1B-P positive structures are represented in (**D**). Note that alignment of fibers with astrocytic processes is always better in ChABC treated animals, although the difference is minimal at 2 weeks post-injury. GM, grey matter; WM, white matter. *$p < 0.05$; **$p < 0{,}01$. Bar is 45 μm. Color image is available online at www.liebertpub.com/neu

the glial scar. Under ChABC treatment, GFAP IR was less intense than in untreated animals (Fig. 2B).

At 2 weeks post-injury, the glial scar was well established in untreated animals,[45] exhibiting a dense GFAP IR processes network even around smaller cavities of secondary injury (Fig. 3A), whereas in ChABC-treated animals (Fig. 3B), the network formed around the cavity was less compact, and most astrocyte processes remained oriented toward the lesion epicenter. At 4 weeks post-injury, a compact glial scar was observed all around the cavity in untreated (Fig. 4A), or P-ase-treated animals (Supplementary Fig. S1; see online supplementary material at ftp.liebertpub.com), but was found only at some restricted locations in ChABC-treated animals (Fig. 4B). Under ChABC treatment, astrocyte remodeling indeed continues at long term. Thus, at later stages (10 weeks post-injury, latest time point analyzed) at the border of the injury site, numerous individual astrocytes could be seen that show almost no sign of reactivity (Supplementary Fig. S2; see online supplementary material at ftp.liebertpub.com).

Axon remodeling after ChABC treatment. To visualize axons, we used an antibody against the phosphorylated form of MAP1B-P, which labels axons undergoing different forms of plasticity in the adult: regeneration in PNS[46] and sprouting in the CNS after a periperal nerve lesion.[17,33] Phosphorylated MAP1B-P is also upregulated in axons undergoing sprouting after SCI.[30]

In untreated or P-ase-treated animals, MAP1B-P-positive fibers at the injury site were disorganized at all time points analyzed (Figs. 2C,E; 3C,E; 4E). During the first 2 weeks post-injury, MAP1B-P-positive fibers were observed within the lesion (Fig. 2C,E; 3C,E), their number being maximal at 2 weeks, before decreasing with time (Fig. 5B), corroborating our previous study using MAP1B-P as a marker revealing the time course of axonal plasticity after SCI.[30] In ChABC-treated animals, the number of MAP1B-P-positive fibers and their extension from the borders toward the center of the injury site were significantly higher than in untreated and P-ase-treated animals, and the peak of fiber density was reached earlier, at 1–2 weeks (Fig. 5B).

An increased MAP1B-P IR was previously described by Galtrey and associates,[17] reflecting an enhancement of axon plasticity in ChABC-treated spinal cord after peripheral nerve injury. Although MAP1B-P-positive fiber numbers slightly decreased between 2 and 4 weeks post-injury, the fiber density within the lesion epicenter was significantly higher in ChABC-treated than in untreated animals at all time points analyzed (Figs. 2D,F for 1 week; 3D,F for 2 weeks; 4D,F for 4 weeks), as summarized in Fig 5B.

Indeed, under ChABC treatment, many axons around the cavity, or within the injury epicenter, displayed an appropriate orientation (i.e., parallel to the rostrocaudal axis; see high magnification in Figs. 3 and 4). This was only rarely observed in untreated animals where the majority of axons stalled at the border of the cavity, and the few axons seen in the injury site were generally associated with astrocyte processes, whose orientation was mostly aberrant (i.e., rather perpendicular to the original direction of the fibers; Fig. 3E).

Correlation between astrocyte processes and axon remodeling. As mentioned above, at all time points post-injury analyzed, we noted that axons oriented toward the lesion site were associated with astrocyte processes, a phenomenon particularly frequent in ChABC-treated animals (Fig. 5). Therefore, we measured the relative areas occupied by GFAP and MAP1B-P labeling within the primary injury site (Fig. 5B; for a schematic representation see the grey area in Fig. 5A). We also evaluated the gross orientation (directionality) of both GFAP and MAP1B-P positive processes at the border of the injury site (Fig. 5D; 5C is a representative confocal microscope image, and three-dimensional videos showing the close association between fibers and GFAP-positive processes are shown in Supplementary data S3; see online supplementary material at ftp.liebertpub.com).

For both treated and untreated animals, the area of the injury site occupied by astrocytic processes was always smaller than the area occupied by axons (Fig. 5B). In untreated animals, GFAP-positive structures occupied $5.3 \pm 3.7\%$ of the total primary injury area at 1 week post-injury, increasing to $7.5 \pm 4.5\%$ at 2 weeks, then staying almost unchanged until 4 weeks post-injury ($7.9 \pm 3\%$). Under ChABC treatment, the area occupied by astrocytic processes was larger ($8.7 \pm 2.6\%$, and $9 \pm 4.3\%$, respectively, at 1 and 2 weeks post-injury), and significantly increased to $15.1 \pm 6.4\%$ ($p < 0.05$) at 4 weeks, indicative of a prolonged period of astrocyte remodeling.

The differences between ChABC-treated and untreated animals concerning the area covered by MAP1B-P positive axons were even much more pronounced, for all three time points analyzed. Thus, at 1 week post-injury, MAP1B-P-positive labeling was found in $34.9 \pm 12.7\%$ of the primary injury area, to be compared with $6.4 \pm 0.9\%$ for untreated animals ($p < 0.05$). The extent of MAP1B-P-labeled areas then slightly decreased with time, to $33 \pm 6.9\%$ at 2 weeks (vs. $18.9 \pm 4.0\%$, $p < 0.05$), and $22.4 \pm 11.5\%$ at 4 weeks (vs. $10.5 \pm 1.6\%$, $p < 0.05$), but still remained twice as high as in untreated animals (Fig. 5B).

A closer look at the zone of entry of axons and astrocytic processes into the injury site revealed a clear association of GFAP labeling with MAP1B-P labeling for both untreated and ChABC-treated animals (compare, for example, at 4 weeks: Fig. 4E and F). The quantitative directionality analysis (Fig. 5D) shows that the orientation of GFAP-positive processes entering the injury site was very similar to that of MAP1B-P-positive fibers.

This phenomenon was more pronounced in ChABC-treated than in untreated animals (Fig. 5D). Thus, the deviation (angle) between the gross trajectories of GFAP-positive astrocytic processes and MAP1B-P-positive axons at the primary injury margin was 7 ± 2.6 degrees for untreated animals at 1 week post-injury, compared with only 2 ± 2 degrees after ChABC treatment ($p < 0.05$). At 2 weeks, the difference between untreated and treated animals was less pronounced (2.7 ± 3.2 degrees and 2.3 ± 0.6 degrees, respectively), but was again significant at 4 weeks (4.1 ± 3 degrees for untreated, vs. 1.1 ± 0.4 degrees for ChABC-treated animals; $p < 0.05$).

Overall, in untreated animals, a good alignment between gross trajectories of fibers and astrocytic processes was observed only at 2 weeks post-injury, while in ChABC-treated animals, the correlation between the two trajectories was always greater, even at later time points post-injury (see Discussion).

These findings show that treatment of SCI with ChABC modifies astrogliosis, while at the same time extending the period of astrocyte remodeling (up to 4 weeks). Further, astrocyte processes that are oriented toward the lesion are associated with remodeling axons at the zone of entry into the damaged tissue. This correlation is enhanced after ChABC treatment.

Influence of ChABC treatment on neoangiogenesis and organization of laminin-positive blood vessel BM

Traumatic SCI inevitably leads to BBB breakdown and vascular network damage, which are followed by neoangiogenesis (for review, see Oudega[47]). To determine if vascular remodeling after SCI is modified by ChABC treatment, we first examined both pre-existing

and newly forming microvasculature through labeling for laminin (to reveal the BM) and RECA-1, a pan-endothelial cell marker.

In intact (control) animals, as well as in undamaged tissue distant from the primary injury site, all laminin-positive structures tightly colocalized with RECA-1 labeling within the same blood vessels, revealing a normal microvasculature and an intact BM (Fig. 6A–C) After SCI, in both untreated and ChABC-treated animals, RECA-1 IR diminished at the injury epicenter during the first week (not shown), then partially reappeared during the second week post-SCI (Fig. 6E,F,H,I), revealing multiple pathological aspects of the intrinsic neoangiogenesis, consistent with previous reports.[11,42,48–50] During these two weeks, ChABC treatment did not appear to modify the density or the labeling of RECA-1 positive blood vessels (Fig. 6).

In lesioned untreated animals, the number of RECA-1 positive vessels was lower than laminin IR would have suggested: in fact, laminin labeled tubes did not always contain endothelial cells (Fig. 6F,L), in accordance with previous results.[11,42] Indeed, at all time points analyzed, laminin IR was strongly increased at the injury site and in adjacent tissue, revealing the extent of the lesion (Fig. 6D,F,J,L). In ChABC-treated animals, laminin IR was comparable to that seen in untreated animals only during the first 2 weeks (Fig. 6G, I). At later time points (4 weeks), the tissular distribution of laminin showed a good correlation with RECA-1 positive blood vessels (Fig. 6M-O; compare with the situation in untreated animals, Fig. 6J-L). Further, we noticed that MAP1B-P–positive axons were often closely apposed to laminin-positive tubules (Supplementary data S4; see online supplementary material at ftp.liebertpub.com), suggesting a role of blood vessels in axonal growth, as previously shown by live imaging in adult rat.[51]

Laminin antibodies also labeled hypertrophied blood vessels, mainly within the scar surrounding the injury site (Fig. 7A), as we had reported previously.[12] For some of them, a separation of their

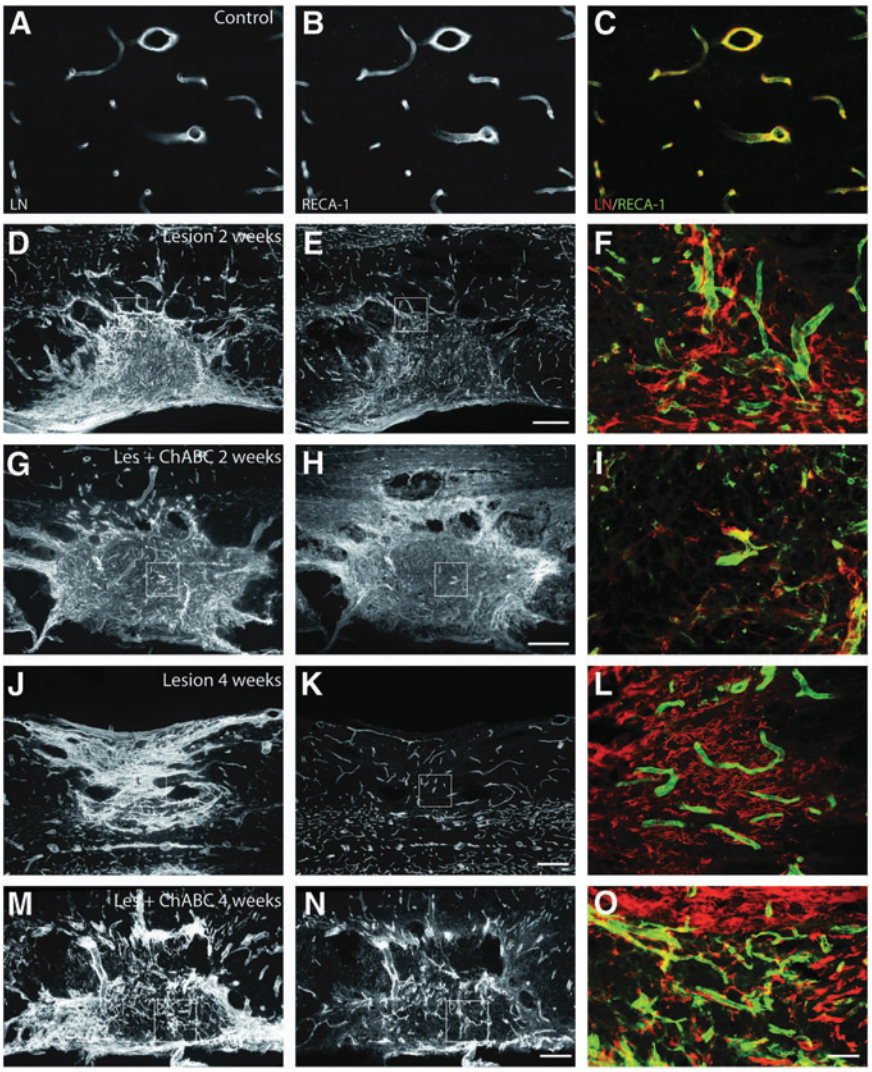

FIG. 6. Evolution of immunolabeling for laminin (LN; left column, red in merge panels), and rat endothelial cell antigen (RECA-1) (middle column, green in merge panels) on spinal cord sections from lesioned untreated (Lesion) and chondroitinase ABC (ChABC)-treated (Les + ChABC) animals, compared with intact (control) animals (A,B, merge image in C). (D–I) 2 weeks, (J–0) 4 weeks post-injury; (D–F, J–L) untreated, (G–I, M–O) ChABC-treated animals. Note that within the injury site, RECA-1–positive blood vessels are less frequent than laminin-immunoreactivity would have suggested. At 4 weeks after ChABC treatment, LN shows important colocalization with RECA-1. F,I,L,O are higher magnification merge images of insets within the same row. Bars: A–C,F,I,L,O, 30 μm; D,E,G,H,J,K,M,N, 200 μm. Color image is available online at www.liebertpub.com/neu

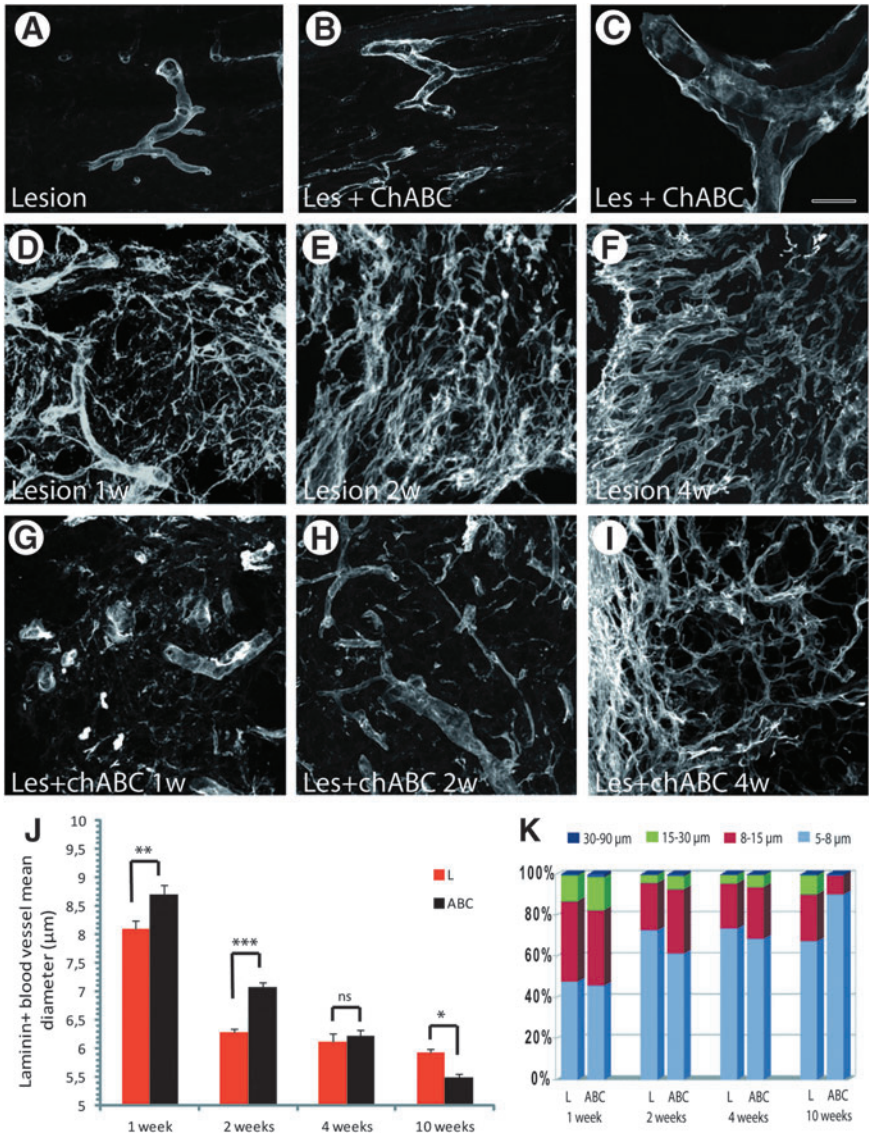

FIG. 7. Analysis of laminin-positive vascular basement membranes (BM). Compared with spinal cord injury (SCI) without treatment (**A**), after chondroitinase ABC (ChABC) treatment, splitting of laminin-positive BM is frequently seen on medium-sized (**B**) and hypertrophhied (**C**, confocal image) blood vessels. (**D–F**): After SCI in untreated animals, laminin is not only found in vascular BM, but high amounts of laminin-positive extracellular matrix deposits are seen at the injury site that persist throughout the period analyzed, shown here for 1 (**D**), 2 (**E**), and 4 (**F**) weeks post-injury. After ChABC treatment, these deposits are decreased (**G–I**). (**J**) Quantification of mean diameters of laminin-positive tubular structures shows a significant shift toward larger diameters in ChABC-treated compared with untreated animals at 1 and 2 weeks post-injury, while this tendency is inversed at 10 weeks post-injury. Error bars indicate standrd error of the mean. (**K**) Quantification of the size distributions of laminin-positive tubular structures, classified into four groups: 5–8 μm (small size), 8–15 μm (medium size), 15–30 μm (big size), and 30–90 μm (huge size) diameter. During the first 2 weeks post-injury, tubular structures of very large diameter are more frequent in ChABC-treated (ABC) than in untreated specimens (L), but at 10 weeks, the number of small vessels is higher for ChABC-treated than for untreated animals. Bars: A,B: 80 μm; C: 15 μm, D–F:80 μm. Color image is available online at www.liebertpub.com/neu

BM into an inner endothelial and an outer perivascular BM layer was observed.[14] Laminin labeling intensity and the number of hypertrophied blood vessels decreased with time and distance from the injury site.

In ChABC-treated animals, the changes in blood vessel morphology were rather striking (Figs. 6, 7). First, laminin-positive hypertrophied blood vessels with abnormal morphology, often tortuous and of irregular diameter, were more numerous than in lesioned untreated animals (Fig. 7B). In addition, within the lesion site, a large number of blood vessels showed detached or duplicated BM (Fig. 7C). Second, at the injury site, laminin also labeled numerous small tubular streamers negative for RECA-1, resembling ECM deposits, as described previously.[11] These latter were observed in untreated animals at all time points (Fig. 6D,F,J,L; 7D–F), and their density remained unchanged. Under ChABC treatment, the density of these streamers was comparatively lower at all time points analyzed (Fig. 6G,I,M,O, 7G–I). Thus, these observations indicate that by cleaving CSPG GAG chains, ChABC obviously modifies not only blood vessel BM, but also blood vessel-independent laminin deposits.

To better investigate the differences in structural remodeling of vessels between ChABC-treated and untreated animals, we evaluated potential differences in luminal diameter by performing a

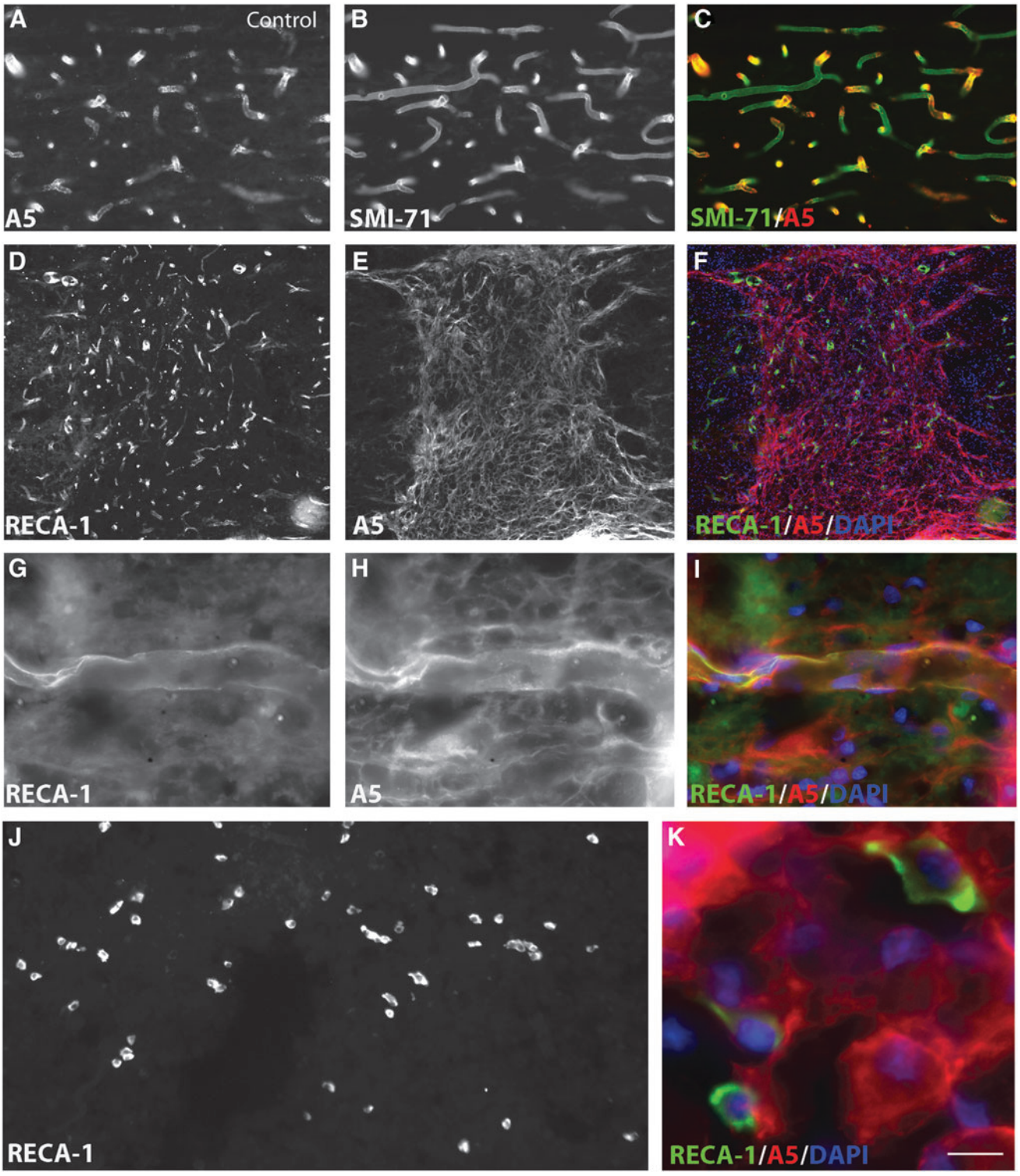

FIG. 8. (**A–C**) AHNAK (A5) double immunostaining with SMI-71 in intact control animals, showing that all mature SMI-71 positive blood vessels are labeled with AHNAK antibody. (**D-I**) Co-immunostaining of AHNAK with rat endothelial cell antigen (RECA)-1 positive vessels is also found within the lesion site of chondroitinase ABC (ChABC)-treated animals 4 weeks post-injury (D–F, overview over the lesion site; G–I, higher magnification of an individual vessel). (**J**) RECA-1 labeling of the injury site, in ChABC-treated animals, 4 weeks post-injury. (**K**) Higher magnification of inset, with triple labeling for RECA-1, AHNAK, and 4',6-diamidino-2-phenylindole (DAPI, blue, nuclei) showing that numerous RECA-1–positive individual endothelial cells in the injury are also expressing AHNAK. Bar: A–C: 25 μm; D–F: 150 μm; G–I: 16 μm; J: 65 μm; K: 11 μm. Color image is available online at www.liebertpub.com/neu

morphometric analysis of laminin-positive tubular structures. For this, only structures that were also positive for RECA-1 were taken into account (for example, see supplementary Fig. S5). At 1 and 2 weeks post-injury, mean diameters of laminin-positive tubular structures were larger in ChABC-treated (ABC) than in untreated animals (L) (Fig. 7J; 1 week: 8.71 μm $\pm$ 0.166 in ChABC animals vs. 8.09 μm $\pm$ 0.147 in L, $p < 0.001$; 2 weeks: 7.08 μm $\pm$ 0.086 in ChABC vs. 6.29 μm $\pm$ 0.60 in L, $p < 0.0001$), and in addition, tubular diameters showed a greater variability. At later time points, the situation was progressively inverted. Thus, at 4 weeks, mean diameters were almost identical for treated and untreated animals (Fig. 7J; 6.23 μm $\pm$ 0.063 in ChABC-treated vs. 6.12 μm $\pm$ 0.059 in L), and at 10 weeks post-injury, the mean diameter of laminin-positive tubular structures in ChABC-treated animals became significantly smaller than in untreated animals (Fig. 7J; 5.49 μm $\pm$ 0.081 in ChABC-treated vs. 5.93 μm $\pm$ 0.118 in L; $p < 0.005$).

These modifications in microvessel size are clearly illustrated by the graph in Fig. 7K, representing a comparison of microvessel size distribution frequencies between ChABC-treated and untreated animals. To this end, laminin-positive blood vessel-like structures were divided into four groups (5–8 μm, small size; 8–15 μm, medium size; 15–30 μm, big; 30–90 μm, huge), similar to the distribution chart proposed by Ormandzhieva.[36] In untreated animals, the percentage of small vessel-like structures increased from 48% at 1 week to 73% at 2 weeks, to remain stable at approximately 70% until 10 weeks post-injury, while values for medium-sized structures decreased from 39% at 1 week to 22–24% at later time points. Big-sized tubular structures initially constituted 13% of the population and then decreased to 4–9% between 2 and 10 weeks post-injury. In ChABC-treated lesioned tissue, the percentage of small laminin-positive vessels (45%) was initially similar to that of untreated animals, then gradually increased from 62% at 2 weeks to 90% at 10 weeks post-injury. The numbers of medium- and big-sized laminin-positive tubular structures dropped sharply from 35% and 19% respectively at 1 week to only 9% (vs. 23% without treatment), and 1%, respectively (vs. 9% for untreated animals) at 10 weeks.

To summarize, these findings show that ChABC treatment affects laminin distribution, resulting in a disruption of blood vessel basement membrane during the first weeks post-injury. In contrast, increased laminin staining at later time points is more directly correlated with newly formed blood vessels than in untreated animals, and the size distribution of these vessels tends to be closer to that found in intact tissue.[10,11] Accordingly, at 4 weeks post-injury, we observed numerous individual RECA-1 positive cells in the lesion site in ChABC-treated animals that were also positive for AHNAK immunolabeling (Fig. 8G,K), a phenomenon rather absent in untreated animals. These observations suggest that neoangionesis is prolonged, or more vigorous, in ChABC-reated animals.

Next, we compared the presence of newly formed mature vasculature between untreated and treated animals through immunolabeling for SMI-71 (Fig. 9), a marker for mature blood vessels.[11] During the first 2 weeks post-injury, the injury epicenter remained almost devoid of mature SMI-71 positive blood vessels, both in treated and untreated animals. Occasionally, from 2 weeks on, a few SMI-71 positive vessels could be detected in the lesion epicenter, and within the surrounding scar. At 4 weeks post-injury, SMI-71 positive vessels are again present within, and around the primary lesion site, without any obvious difference between the two experimental conditions (Fig. 9).

We further analyzed the spatiotemporal distribution pattern of the TJ-associated protein ZO-1, together with that of AHNAK, shown to colocalize with ZO-1 in ECs with BBB properties in intact CNS.[15,52] In both intact and injured spinal cord, AHNAK-IR is found within blood vessels that are also positive for either SMI 71

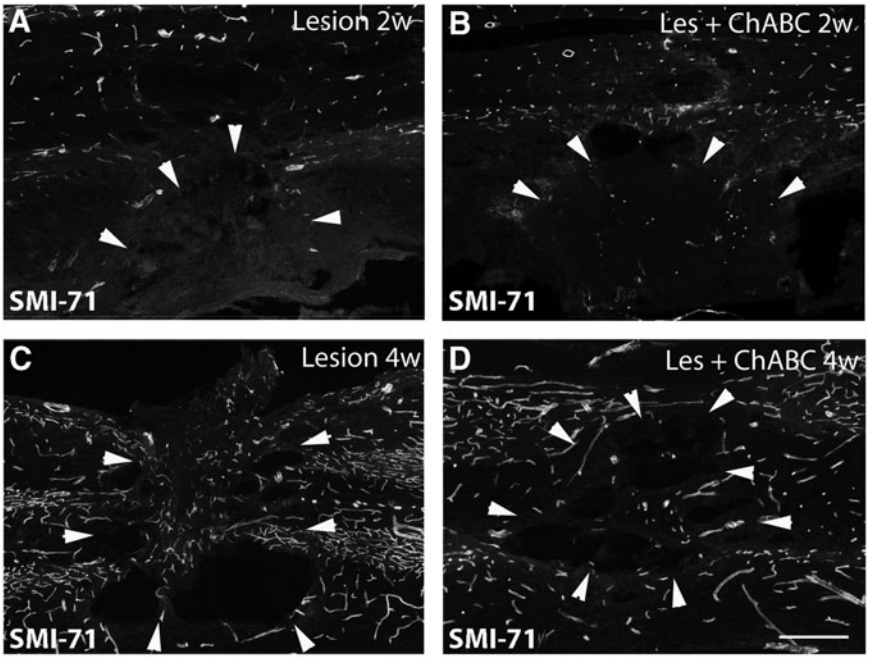

FIG. 9. SMI-71 immunolabeling on spinal cord sections at 2 weeks (**A,B**), and 4 weeks (**C,D**) post-injury; (A,C) untreated, (B,D) chondroitinase ABC (ChABC)-treated animals. Two weeks after the lesion, almost no mature blood vessels are observed within the injury site, both in untreated and treated animals. At 4 weeks, some mature blood vessels reappear in the injury site in both untreated and treated animals. Bars: 95 μm.

(intact tissue, Fig. 8A–C,) or RECA-1 (injured tissue in Fig. 8G–I) immunolabeling. Interendothelial tight junctions contribute to normal vascular function and to the tightly regulated barrier properties of CNS vasculature[53]; see references in [42]. In association with BBB breakdown after a traumatic lesion, blood vessel TJ are compromised, as reflected by altered distribution and decreasing levels of its constituents, such as ZO-1.[42]

Accordingly, in lesioned untreated animals, we observed a rather diffuse ZO-1 labeling during first weeks that, in addition, was also present on some thin structures around the lesion (Fig. 10A,C). In the injury epicenter, only weak ZO-1 labeling was found, which was associated with AHNAK-positive microcavity-forming cells, while being associated with blood vessels at the lesion border (Fig. 10 C,E). At 4 weeks (Fig. 10 G,I) and 10 weeks (not shown), ZO-1 labeling became more pronounced in the injury epicenter, associated with blood vessels, and at appositions between microcavities. Outside the injury, ZO-1 labeling would precisely delineate blood vessels (not shown).

After ChABC treatment, ZO-1 labeling at 2 weeks post-injury appeared more diffuse, with patches at the border of the lesion, rarely seen in untreated animals (Fig. 10B,D). At the lesion epicenter, particularly around microcavities, ZO-1 was almost undetectable (Fig. 10D). At 4 weeks, as in untreated animals, ZO-1 labeling became more intense at the borders of the injury (Fig. 10H). The thin, microcavity-associated ZO-1 positive structures typically seen at the injury center of untreated animals, however, were less obvious in ChABC-treated animals, and appeared more diffuse (Fig. 10H).

Finally, AHNAK is a useful marker to reveal both the extent of the injury and the state of the vasculature modified in consequence to the SCI. We had previously shown that AHNAK is expressed by GFAP-negative cells such as fibroblasts and epithelial cells invading the lesion epicenter, forming a barrier in front of the astrocytic scar. AHNAK staining delineates microcavities filled with ED1-positive macrophages and marks ECs implicated in neoangiogenesis (for details, see Von Boxberg and associates[12]). Lesion-induced *de novo* AHNAK expression was seen in both untreated and ChABC-treated animals. Expression levels increased at later times post-injury, when the majority of AHNAK positive cells were associated with microcavities (Fig. 10E).

The fact that AHNAK is codistributed with laminin both at the BBB and in the spinal cord lesion site[12] in addition to our demonstration that AHNAK is implicated in laminin adhesion of Schwann cells[54] prompted us to suggest an indirect interaction between AHNAK and the BM constituent laminin. Interestingly, although initially we did not detect any obvious differences between the immunostaining intensity of both AHNAK and laminin in the lesion epicenter of ChABC-treated and untreated animals, Western blotting revealed that levels of both proteins were slightly although not significantly lower during the first 2 weeks in ChABC-treated, compared with untreated animals, a tendency that was reversed at 4 weeks post-injury (Fig. 11).

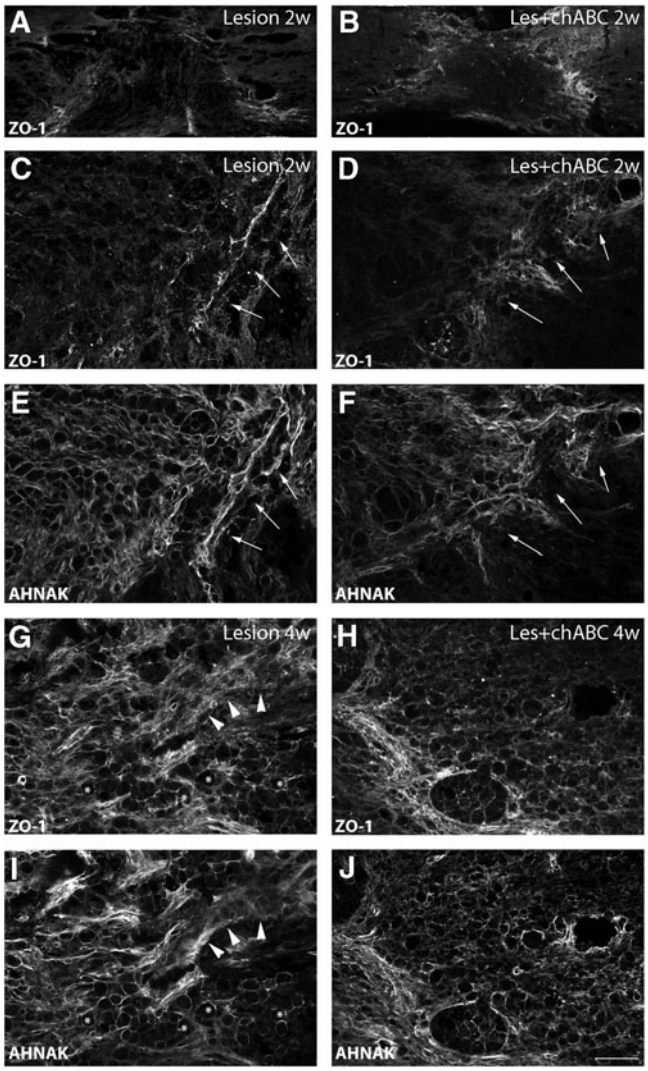

FIG. 10. Tissular distribution of ZO-1 at the lesion site, shown at low (**A,B**) and at high magnification (**C,D** and **G,H**) of spinal cord sections taken at (**A–D**), 2 weeks; (**G,H**), 4 weeks post-injury. **E,F**, and **I,J** show the same sections as in C,D, and G,H, respectively, double immunostained for AHNAK. Left panels represent lesioned untreated (Lesion); right panels, chondroitinase ABC (ChABC)-treated (Les + ChABC) animals. At 2 weeks (A-D), ZO-1 labeling is present at the border of the lesion (arrows in C–F), colocalizing with AHNAK, but within the injury site, it is very weak in untreated animals and hardly detectable in ChABC-treated animals. In addition, under ChABC treatment, ZO-1 labeling at the border of the injury (arrows) appears more diffuse (D). At 4 weeks (G–J), ZO-1 exhibits a distribution pattern quite similar to that of AHNAK, with microcavities (stars) and blood vessels (arrowheads; G,I), but labeling is overall weaker and more diffuse in the lesion epicenter after ChABC treatment (H,J). C and D are higher magnifications of A and B, respectively. Bars: A,B: 160 μm; C–J: 95 μm.

Discussion

ChABC treatment modifies the astrocytic reaction after SCI

Astrocytes are complex, highly differentiated glial cells assuring numerous essential functions within the entire CNS. To all forms of insults to the CNS, including subtle perturbations, astrocytes respond by a process commonly referred to as reactive astrogliosis, involving changes in gene expression and morphology that vary with the nature and severity of the insult. A growing number of reports provide evidence that astrogliosis may exert both beneficial and detrimental effects. In particular, reducing scar formation after a lesion by a knockdown of certain genes expressed by reactive astrocytes or by eliminating proliferating astrocytes appears not suitable as a therapeutic approach. In fact, these studies reveal that the presence of astrocytes at the lesion site is essential for neural

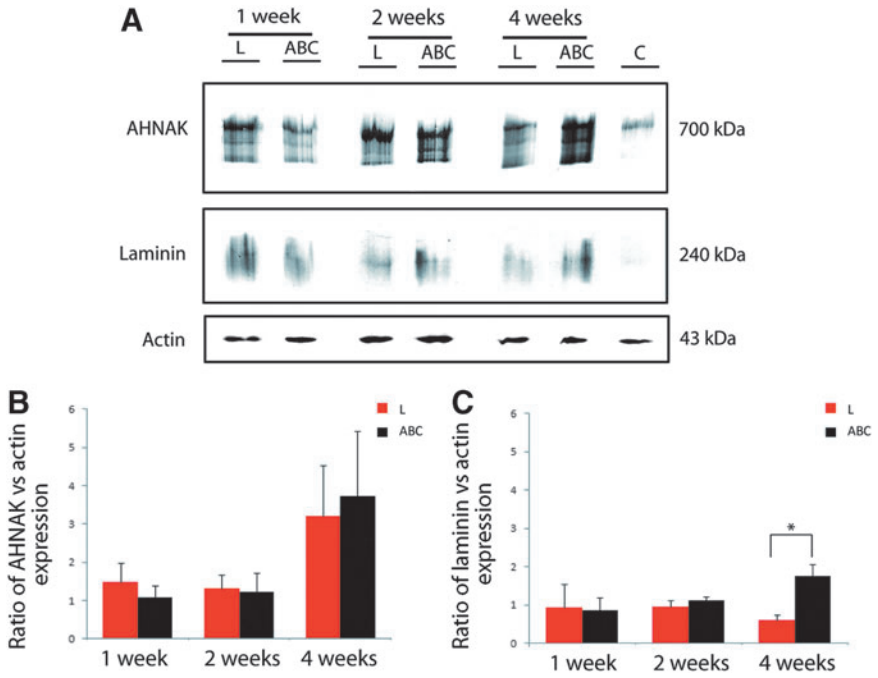

FIG. 11. Western blot analysis of AHNAK and laminin expression at the injury site in untreated (L), and chondroitinase ABC (ChABC)-treated (ABC) animals. (**A**) AHNAK expression increases after spinal cord injury (SCI) compared with intact control (C) animals at 1 week and remains elevated at 2 and 4 weeks post-injury. Laminin expression strongly increases after SCI and stays elevated until 4 weeks post-injury, similar to AHNAK. As shown in graph (**B**), after ChABC treatment, AHNAK expression is slightly decreased at 1 week post-injury, attains similar levels at 2 weeks, and is slightly increased at 4 weeks post-injury compared with untreated animals. (**C**) ChABC treatment has a slight but not significant effect on laminin expression levels during the first 2 weeks, which become significantly stronger ($p < 0.05$) at 4 weeks post-injury. Actin is used as loading control and reference for calculating relative amounts of AHNAK and laminin immunoreactivity. Color image is available online at www.liebertpub.com/neu

protection, and regulation of inflammation (for review, see[55,56] and references therein).

The process of glial scar formation after SCI starts by a hypertrophy of astrocytes, which then proliferate, migrate, differentiate, and create a dense fibrous network that constitutes a physical and chemical barrier to axon outgrowth. The border of a mature scar (i.e., about 2 weeks post-injury) was recently shown to be composed essentially of newly proliferated astrocytes with elongated cell processes.[44] The chemical barrier property of the scar is mainly attributed to increased expression and release of CSPG. Degradation of CSPG by ChABC treatment does indeed result in improved SCI repair, which can be even further enhanced by combinatorial strategies that synergistically promote axonal regeneration and functional recovery.

So far, few studies have addressed the impact of ChABC treatment on astrocyte morphology, and none reported any relevant influence on scar formation,[57,58] excepting the work of Chau and colleagues,[59] who combined ChABC treatment with Schwann cell grafts, which resulted in a decrease of GFAP labeling and stimulation of astrocytic processes entering the graft tissue. Our present study clearly demonstrates that treating the injured spinal cord with ChABC alone was sufficient to achieve the modification of the astrocytic reaction described by Chau and colleagues.[59] Independent of the effect on the morphology of reactive astrocytes described here, Karimi-Abdolrezaee and coworkers[60] recently demonstrated that ChABC treatment, although generally increasing cell proliferation, also reduces differentiation of neural precursor cells into astrocytes, in favor of the oligodendroycte lineage.

The degree of the astrocytic reaction depends on the severity of the insult and can be classified as mild to moderate, up to severe astrogliosis with scar formation (for review, see[55]). After SCI, this graded response can be observed ranging from a mild reaction in segments distal to the injury toward scar formation at the primary lesion site.

Our present study shows that on ChABC treatment, GFAP immunolabeling is decreased and, even more importantly, the number of astrocytes exhibiting thin and long processes oriented toward the lesion site is enhanced. Without treatment, this phenotype could be observed only during the first week post-injury (processes are aligned, and mostly oriented toward the lesion center during the first 5 days post-lesion, before the scar is fully formed[44]). We interpret this effect as a reduction of astrogliosis from severe to moderate, rather than a delay in the astrocytic reaction during the 10-day period of ChABC treatment.

This is supported by our observation that even at rather late time points post-injury (10 weeks), the astrocytic network around the lesion is not as dense as the one seen after SCI without ChABC treatment. After CSPG degradation, individual astrocytes surrounding the injury site can be distinguished, while GFAP-positive processes in untreated SCI appear highly interdigitized. Moreover, as revealed by our quantitative analysis of astrocyte processes oriented toward the lesion, the dynamics of astrocyte remodeling is prolonged up to 4 weeks post-injury, while in untreated animals, completion and stabilization of the glial scar occur earlier, at around 2 weeks, and are accompanied by a major decrease in CSPG expression.

Reactive astrocytes also express various other extracellular matrix components, such as laminin[61,62] and fibronectin,[63] and form a new

glia limitans, associated with a basal lamina demarcating the damaged tissue.[64] Our observations suggest that GAG cleavage on CSPG modifies the ECM organization, allowing for the extension of motile astrocytic processes towards the lesion epicenter.

Association of axon remodeling with astrocytic processes preferentially oriented toward the lesion site after ChABC treatment: who is helping whom?

Our results clearly demonstrate that the repeated intrathecal injections of ChABC at the sacral level are effective in cleaving CSPG GAG side chains at the thoracic lesion site, where they lead to rather extensive axonal remodeling during the first 2 weeks. Thereafter, although remaining significantly higher than in untreated animals, the number of axons within the injury site decreases, suggesting retraction or degeneration of fibers with time after scar formation (for review, see Silver and Miller[4]). Interestingly, we observed that at the border of the injury site, axons and astrocytic processes were rather closely associated, suggestive of a more or less direct interaction; in other words, it appeared as if astrocytic processes would facilitate axonal entry into the injury site.

It has indeed been proposed before that up to a certain level of reactivity, astrocytes are not inhibitory for growing axons[65–68] and might participate in guiding sprouting or regenerating axons in adult CNS, as is the case during development (for review, see Powell and associates[69]). Several mechanisms have been put forward that may account for the stimulation of axon growth in response to ChABC treatment such as an effect on axons themselves (attenuation of receptor-mediated growth inhibition, or of growth inhibitory downstream signaling in response to CSPG), liberation of matrix bound factors permissive for axonal regeneration, or modification of interactions between CSPG and other matrix molecules, like laminin (for review, see Bradbury and Carter[70]).

Although the idea of astrocytes guiding axon remodeling appears the most plausible and is supported by several reports, the experimental model used in the present study does not allow us to exclude that, on the contrary, growing axons might play a role in guiding astrocyte processes. In favor of this latter interpretation, we may cite our observation that axonal plasticity within the lesion was most intense during the 2 first weeks, while astrocyte remodeling continued thereafter and even appeared more important at 4 weeks post-injury in ChABC- treated animals. The correlation between the orientations of axons and astrocyte processes was also most obvious at this time point. Further, this interpretation is corroborated by data demonstrating that during the first days post-injury NG2-positive, metalloprotease (MMP)-secreting cells, rather than astrocytes, invade the lesion site, where they provide a stabilizing substrate for injured axons, thus protecting them against macrophage-mediated die-back.[71]

ChABC treatment modifies revascularization and blood vessel basement membrane morphology

The second major finding of the present study concerns the modification by ChABC treatment of the distribution and, temporarily, the expression of laminin after SCI. Compared with lesioned untreated animals, we observed that blood vessel basement membranes more frequently exhibited a disrupted morphology during the first weeks post-injury, accompanied by slightly, although not significantly decreased laminin immunolabeling and protein levels. In contrast, at later time points (from 4 weeks post-injury on), laminin protein levels were significantly increased, and its tissular distribution was principally associated with newly formed blood vessels, in contrast to the numerous streamers (laminin-rich matrix deposits) characteristic for untreated animals. Further, at 10 weeks post-injury, the size of newly formed vessels was more homogeneous and tended to be closer to that found in intact tissue.

Under ChABC treatment, morphological changes of blood vessels at the injury site and in adjacent tissue differ from those seen in lesioned untreated animals. In particular, vessels initially exhibit hypervariable diameters. The rather high number of hypertrophied vessels is likely to reflect the detachment of their BM, a phenomenon that we frequently observed in treated, but rarely in injured untreated animals. A similar detachment of blood vessel BM has been described as characteristic for tumor blood vessels,[72] diabetic retinopathy,[73] and Alzheimer disease.[74] Only very recently, Takigawa and associates[14] reported that after SCI, blood vessel walls can exhibit a separation of their BM in an inner endothelial, and an outer parenchymal part, although not all blood vessels are concerned.

In vivo analyses had shown that besides its major constituents collagen IV and laminin, blood vessel BM also contains HSPG and CSPG.[6,7] Because CSPG is able to directly bind to laminin, at least *in vitro,*[75–78] cleavage of CSPG in laminin-rich blood vessel BM might well affect the structure of these membranes and increase their detachment and separation. This effect of CSPG degradation appears to also concern blood vessel-independent laminin deposits, because we noted less streamer deposits in treated animals, associated with a slight decrease in laminin protein levels during the first weeks after SCI.

After a traumatic injury of the spinal cord, which is highly vascularized, the lesion epicenter is filled with hemorrhage and edema from the primary insult causing local damage of blood vessels, thereby compromising the blood-spinal cord barrier (BSCB). The resulting ischemia and inflammation then contribute to secondary anatomical damage and neurological deficits. This initial mechanical insult provokes a dramatic death of endothelial cells within the first 24 hours,[48] and vessel density continues to decrease, with only very few, if any, vessels observable at the injury epicenter at 1 week post-injury[42,48,50] (present data). Then, local angiogenesis starts within the injured spinal cord tissue, which is a normal response to trauma[11,42,48,50] (present data). Although there is significant angiogenic growth during early phases post-injury, the newly formed vessels (revealed here by RECA-1 immunolabeling) may not be fully functional. Compared with intact tissue, the density of mature vessels remains low; only part of the newly grown vessels become stable and functionally integrated blood vessels,[42] as shown here by SMI-71 immunolabeling.

ChABC treatment does not seem to modify the initial phase of vasculature remodeling after SCI. At 4 weeks post-injury, however, we noted that the number of individual RECA-1-positive endothelial cells was higher in the injury site of ChABC-treated than of untreated animals, indicative of a prolonged period of neoangiogenesis and blood vessel maturation. In fact, recruitment of endothelial cells after ChABC treatment may be facilitated by the physical and molecular remodeling of the scar, as well as the reduction in cavity volume[79] (our own observation, not shown).

Initiation of angiogenesis and revascularization at the injury epicenter correlates with increased BSCB permeability, lasting up to 21 days in mouse and 28 days in rat (for review, see Ng and associates[80] and referencess therein). This period is characterized by the lack of functional tight junctions between endothelial cells, the main structures assuring the barrier properties.[81] Even if the major components of TJ are occludin and claudin proteins,

cytoplasmic accessory proteins such as zonula occludens-1 (*cf.* our ZO-1 immunolabeling) are important for TJ anchoring in the membrane and as support structure for signal transduction proteins.[82] Loss of ZO-1, or its dissociation from the junctional complex, was shown to be associated with increased barrier permeability.[42,83–85]

We noted that during the first week post-injury, probably related to the pronounced BM detachment, ZO-1 distribution in the lesion epicenter appeared more strongly affected after ChABC treatment. Note that at this time post-injury, we also observed a slight decrease not only in laminin, but also in AHNAK protein, which colocalizes with ZO-1 at TJs.[15] Thereafter, however, ZO-1 labeling appeared comparable to untreated animals, associated with newly formed vessels.

To evaluate BSCB permeability, we analyzed the extravasation of IgG at all time points post-injury and found that ChABC treatment does not affect BSCB restoration after SCI (data not shown); in fact, IgG extravasation was slightly, albeit not significantly, decreased in ChABC-tretaed animals, probably reflecting the decreased cavity size.[79]

Finally, the present study further reveals the spatiotemporal changes in immunolabeling for AHNAK protein, the levels of which are highly increased after SCI, corroborating our previous study.[12] Upregulation of AHNAK after SCI is associated not only with endothelial cells undergoing revascularization, but also with non-endothelial cells in the lesion epicenter that form microcavities, harboring mainly IB4- and ED1-positive inflammatory cells in their lumen.[12] These microcavity-forming cells are likely to be of epithelial origin, and the observed codistribution of AHNAK and ZO-1 at sites of intercellular contact suggests their interaction via TJ. After ChABC treatment, we found that in microcavities, immunolabeling for ZO-1, although progressively returning to its normal aspect on newly formed blood vessels, remained more diffuse than in untreated animals, reflecting an additional modification of cellular remodeling in the lesion.

Conclusion

Our study corroborates and extends previous studies reporting a beneficial effect of ChABC treatment on neuroprotection and axonal plasticity after SCI (for review, see Bradbury and Carter[70]). Thus, we demonstrate for the first time that ChABC treatment reduces not only the chemical, but also the physical barrier to axon remodeling, while at the same time increasing astrocyte dynamics and remodeling, in a way allowing for a close association between growing axons and astrocytic processes. Moreover, the process of revascularization of the lesion site appears more efficient at long term, because ChABC treatment ultimately favors formation of neovessels exhibiting a BM closely resembling that of vessels in intact tissue.

Despite these beneficial effects, ChABC treatment alone is not sufficient for a complete repair. A combination with other therapeutic strategies, however, is indeed very promising, as shown by recent studies that have associated ChABC treatment with implantation of biological scaffolds, conditioning lesions, peripheral nerve graft, supplementation with growth factors, transplantation of stem cells, and last but not least, rehabilitation.[25,60,86–88]

Acknowledgments

This work was supported by Centre National de la Recherche Scientifique (CNRS), Institut National de la Santé et de la Recherche Médicale (INSERM), Université Pierre et Marie Curie (UPMC), Institut de Recherche pour la Moelle Epinière et l'Encéphale (IRME), and for PhD fellowships to U Milbreta, the Ministère de la Recherche et de l'Enseignement Supérieur and the Association Demain Debout. We thank Dr. Isabelle Dusart for careful reading and helpful comments on this manuscript.

Author Disclosure Statement

No competing financial interests exist.

References

1. Fitch, M.T., and Silver, J. (1997). Activated macrophages and the blood-brain barrier: inflammation after CNS injury leads to increases in putative inhibitory molecules. Exp. Neurol. 148, 587–603.
2. Rhodes, K.E., and Fawcett, J.W. (2004). Chondroitin sulphate proteoglycans: preventing plasticity or protecting the CNS? J. Anat. 204, 33–48.
3. Rhodes, K.E., Raivich, G., and Fawcett, J.W. (2006). The injury response of oligodendrocyte precursor cells is induced by platelets, macrophages and inflammation-associated cytokines. Neuroscience 140, 87–100.
4. Silver, J., and Miller, J.H. (2004). Regeneration beyond the glial scar. Nat. Rev. Neurosci. 5, 146–156.
5. Sofroniew, M. V. (2000). Astrocyte failure as a cause of CNS dysfunction. Mol. Psychiatry 5, 230–232.
6. Couchman, J.R., Caterson, B., Christner, J.E., and Baker, J.R. (1984). Mapping by monoclonal antibody detection of glycosaminoglycans in connective tissues. Nature 307, 650–652.
7. Schmidley, J.W., and Blue, P. (1988). Isolation of glycosaminoglycans from basement membranes of brain microvessels. Brain Res. Bull. 20, 27–31.
8. Noble, L.J., and Wrathall, J.R. (1989). Correlative analyses of lesion development and functional status after graded spinal cord contusive injuries in the rat. Exp. Neurol. 103, 34–40.
9. Popovich, P.G., Horner, P.J., Mullin, B.B., and Stokes, B.T. (1996). A quantitative spatial analysis of the blood-spinal cord barrier. I. Permeability changes after experimental spinal contusion injury. Exp. Neurol. 142, 258–275.
10. Blight, A.R. (1991). Morphometric analysis of a model of spinal cord injury in guinea pigs, with behavioral evidence of delayed secondary pathology. J. Neurol. Sci. 103, 156–171.
11. Loy, D.N., Crawford, C.H., Darnall, J.B., Burke, D.A., Onifer, S.M., and Whittemore, S.R. (2002). Temporal progression of angiogenesis and basal lamina deposition after contusive spinal cord injury in the adult rat. J. Comp. Neurol. 445, 308–324.
12. Von Boxberg, Y., Salim, C., Soares, S., Baloui, H., Alterio, J., Ravaille-Veron, M., and Nothias, F. (2006). Spinal cord injury-induced upregulation of AHNAK, expressed in cells delineating cystic cavities, and associated with neoangiogenesis. Eur. J. Neurosci. 24, 1031–1041.
13. Jaeger, C.B., and Blight, A.R. (1997). Spinal cord compression injury in guinea pigs: structural changes of endothelium and its perivascular cell associations after blood-brain barrier breakdown and repair. Exp. Neurol. 144, 381–399.
14. Takigawa, T., Yonezawa, T., Yoshitaka, T., Minaguchi, J., Kurosaki, M., Tanaka, M., Sado, Y., Ohtsuka, A., Ozaki, T., and Ninomiya, Y. (2010). Separation of the perivascular basement membrane provides a conduit for inflammatory cells in a mouse spinal cord injury model. J. Neurotrauma 27, 739–751.
15. Gentil, B.J., Benaud, C., Delphin, C., Remy, C., Berezowski, V., Cecchelli, R., Feraud, O., Vittet, D., and Baudier, J. (2005). Specific AHNAK expression in brain endothelial cells with barrier properties. J. Cell. Physiol. 203, 362–371.
16. Carulli, D., Pizzorusso, T., Kwok, J.C.F., Putignano, E., Poli, A., Forostyak, S., Andrews, M.R., Deepa, S.S., Glant, T.T., and Fawcett, J.W. (2010). Animals lacking link protein have attenuated perineuronal nets and persistent plasticity. Brain 133, 2331–2347.
17. Galtrey, C.M., Asher, R.A., Nothias, F., and Fawcett, J.W. (2007). Promoting plasticity in the spinal cord with chondroitinase improves functional recovery after peripheral nerve repair. Brain 130, 926–939.
18. Barritt, A.W., Davies, M., Marchand, F., Hartley, R., Grist, J., Yip, P., McMahon, S.B., and Bradbury, E.J. (2006). Chondroitinase ABC promotes sprouting of intact and injured spinal systems after spinal cord injury. J. Neurosci. 26, 10856–10867.

19. Bradbury, E.J., Moon, L.D., Popat, R.J., King, V.R., Bennett, G.S., Patel, P.N., Fawcett, J.W., and McMahon, S.B. (2002). Chondroitinase ABC promotes functional recovery after spinal cord injury. Nature 416, 636–640.
20. Caggiano, A.O., Zimber, M.P., Ganguly, A., Blight, A.R., and Gruskin, E.A. (2005). Chondroitinase ABCI improves locomotion and bladder function following contusion injury of the rat spinal cord. J. Neurotrauma 22, 226–239.
21. Fouad, K., Schnell, L., Bunge, M.B., Schwab, M.E., Liebscher, T., and Pearse, D.D. (2005). Combining Schwann cell bridges and olfactory-ensheathing glia grafts with chondroitinase promotes locomotor recovery after complete transection of the spinal cord. J. Neurosci. 25, 1169–1178.
22. Massey, J.M., Hubscher, C.H., Wagoner, M.R., Decker, J.A., Amps, J., Silver, J., and Onifer, S.M. (2006). Chondroitinase ABC digestion of the perineuronal net promotes functional collateral sprouting in the cuneate nucleus after cervical spinal cord injury. J. Neurosci. 26, 4406–14.
23. Tom, V.J., Kadakia, R., Santi, L., and Houlé, J.D. (2009). Administration of chondroitinase ABC rostral or caudal to a spinal cord injury site promotes anatomical but not functional plasticity. J. Neurotrauma 26, 2323–2333.
24. García-Alías, G., Lin, R., Akrimi, S.F., Story, D., Bradbury, E.J., and Fawcett, J.W. (2008). Therapeutic time window for the application of chondroitinase ABC after spinal cord injury. Exp. Neurol. 210, 331–338.
25. Wang, D., Ichiyama, R.M., Zhao, R., Andrews, M.R., and Fawcett, J.W. (2011). Chondroitinase combined with rehabilitation promotes recovery of forelimb function in rats with chronic spinal cord injury. J. Neurosci. 31, 9332–9344.
26. Tester, N.J., and Howland, D.R. (2008). Chondroitinase ABC improves basic and skilled locomotion in spinal cord injured cats. Exp. Neurol. 209, 483–496.
27. Houle, J.D., Tom, V.J., Mayes, D., Wagoner, G., Phillips, N., and Silver, J. (2006). Combining an autologous peripheral nervous system ''bridge'' and matrix modification by chondroitinase allows robust, functional regeneration beyond a hemisection lesion of the adult rat spinal cord. J. Neurosci. 26, 7405–7415.
28. Alilain, W.J., Horn, K.P., Hu, H., Dick, T.E., and Silver, J. (2011). Functional regeneration of respiratory pathways after spinal cord injury. Nature 475, 196–200.
29. Zhao, R.-R., Andrews, M.R., Wang, D., Warren, P., Gullo, M., Schnell, L., Schwab, M.E., and Fawcett, J.W. (2013). Combination treatment with anti-Nogo-A and chondroitinase ABC is more effective than single treatments at enhancing functional recovery after spinal cord injury. Eur. J. Neurosci. 38,2946–2961.
30. Soares, S., Barnat, M., Salim, C., Von Boxberg, Y., Ravaille-Veron, M., and Nothias, F. (2007). Extensive structural remodeling of the injured spinal cord revealed by phosphorylated MAP1B in sprouting axons and degenerating neurons. Eur. J. Neurosci. 26, 1446–1461.
31. Thibault, K., Van Steenwinckel, J., Brisorgueil, M.J., Fischer, J., Hamon, M., Calvino, B., and Conrath, M. (2008). Serotonin 5-HT2A receptor involvement and Fos expression at the spinal level in vincristine-induced neuropathy in the rat. Pain 140, 305–322.
32. Nothias, F., Fischer, I., Murray, M., Mirman, S., and Vincent, J.D. (1996). Expression of a phosphorylated isoform of MAP1B is maintained in adult central nervous system areas that retain capacity for structural plasticity. J. Comp. Neurol. 368, 317–334.
33. Soares, S., Von Boxberg, Y., Lombard, M.C., Ravaille-Veron, M., Fischer, I., Eyer, J., and Nothias, F. (2002). Phosphorylated MAP1B is induced in central sprouting of primary afferents in response to peripheral injury but not in response to rhizotomy. Eur. J. Neurosci. 16, 593–606.
34. Boxberg, Y.V. (1988). Protein analysis on two-dimensional polyacrylamide gels in the femtogram range: use of a new sulfur-labeling reagent. Anal. Biochem. 169, 372–375.
35. Schindelin, J., Arganda-Carreras, I., Frise, E., Kaynig, V., Longair, M., Pietzsch, T., Preibisch, S., Rueden, C., Saalfeld, S., Schmid, B., Tinevez, J.-Y., White, D.J., Hartenstein, V., Eliceiri, K., Tomancak, P., and Cardona, A. (2012). Fiji: an open-source platform for biological-image analysis. Nat. Methods 9, 676–82.
36. Ormandzhieva, V.K. (2011). Rat choroid plexus blood vessels: morphometric characteristics. Med. Data 3, 229–232.
37. Asher, R.A., Morgenstern, D.A., Fidler, P.S., Adcock, K.H., Oohira, A., Braistead, J.E., Levine, J.M., Margolis, R.U., Rogers, J.H., and Fawcett, J.W. (2000). Neurocan is upregulated in injured brain and in cytokine-treated astrocytes. J. Neurosci. 20, 2427–2438.
38. Asher, R.A., Morgenstern, D.A., Shearer, M.C., Adcock, K.H., Pesheva, P., and Fawcett, J.W. (2002). Versican is upregulated in CNS injury and is a product of oligodendrocyte lineage cells. J. Neurosci. 22, 2225–2236.
39. Jones, L.L., Margolis, R.U., and Tuszynski, M.H. (2003). The chondroitin sulfate proteoglycans neurocan, brevican, phosphacan, and versican are differentially regulated following spinal cord injury. Exp. Neurol. 182, 399–411.
40. McKeon, R.J., Schreiber, R.C., Rudge, J.S., and Silver, J. (1991). Reduction of neurite outgrowth in a model of glial scarring following CNS injury is correlated with the expression of inhibitory molecules on reactive astrocytes. J. Neurosci. 11, 3398–3411.
41. Tang, X., Davies, J.E., and Davies, S.J. (2003). Changes in distribution, cell associations, and protein expression levels of NG2, neurocan, phosphacan, brevican, versican V2, and tenascin-C during acute to chronic maturation of spinal cord scar tissue. J. Neurosci. Res. 71, 427–44.
42. Benton, R.L., Maddie, M.A., Minnillo, D.R., Hagg, T., and Whittemore, S.R. (2008). Griffonia simplicifolia isolectin B4 identifies a specific subpopulation of angiogenic blood vessels following contusive spinal cord injury in the adult mouse. J. Comp. Neurol. 507, 1031–1052.
43. Ozerdem, U., Grako, K.A., Dahlin-Huppe, K., Monosov, E., and Stallcup, W.B. (2001). NG2 proteoglycan is expressed exclusively by mural cells during vascular morphogenesis. Dev. Dyn. 222, 218–227.
44. Wanner, I.B., Anderson, M.A., Song, B., Levine, J., Fernandez, A., Gray-Thompson, Z., Ao, Y., and Sofroniew, M.V. (2013). Glial scar borders are formed by newly proliferated, elongated astrocytes that interact to corral inflammatory and fibrotic cells via STAT3-dependent mechanisms after spinal cord injury. J. Neurosci. 33, 12870–12886.
45. Berry, M., Maxwell, W.L., Logan, A., Mathewson, A., McConnell, P., Ashhurst, D.E., and Thomas, G.H. (1983). Deposition of scar tissue in the central nervous system. Acta Neurochir. Suppl. (Wien) 32, 31–53.
46. Ma, D., Nothias, F., Boyne, L.J., and Fischer, I. (1997). Differential regulation of microtubule-associated protein 1B (MAP1B) in rat CNS and PNS during development. J. Neurosci. Res. 49, 319–332.
47. Oudega, M. (2012). Molecular and cellular mechanisms underlying the role of blood vessels in spinal cord injury and repair. Cell Tissue Res. 349, 269–288.
48. Casella, G.T., Marcillo, A., Bunge, M.B., and Wood, P.M. (2002). New vascular tissue rapidly replaces neural parenchyma and vessels destroyed by a contusion injury to the rat spinal cord. Exp. Neurol. 173, 63–76.
49. Casella, G.T., Bunge, M.B., and Wood, P.M. (2006). Endothelial cell loss is not a major cause of neuronal and glial cell death following contusion injury of the spinal cord. Exp. Neurol. 202, 8–20.
50. Whetstone, W.D., Hsu, J.Y., Eisenberg, M., Werb, Z., and Noble-Haeusslein, L.J. (2003). Blood-spinal cord barrier after spinal cord injury: relation to revascularization and wound healing. J. Neurosci. Res. 74, 227–239.
51. Dray, C., Rougon, G., and Debarbieux, F. (2009). Quantitative analysis by in vivo imaging of the dynamics of vascular and axonal networks in injured mouse spinal cord. Proc. Natl. Acad. Sci. U. S. A. 106, 9459–9464.
52. Gentil, B.J., Delphin, C., Benaud, C., and Baudier, J. (2003). Expression of the giant protein AHNAK (desmoyokin) in muscle and lining epithelial cells. J. Histochem. Cytochem. 51, 339–348.
53. Bazzoni, G., and Dejana, E. (2004). Endothelial cell-to-cell junctions: molecular organization and role in vascular homeostasis. Physiol. Rev. 84, 869–901.
54. Salim, C., Boxberg, Y.V, Alterio, J., Féréol, S., and Nothias, F. (2009). The giant protein AHNAK involved in morphogenesis and laminin substrate adhesion of myelinating Schwann cells. Glia 57, 535–549.
55. Sofroniew, M.V. (2009). Molecular dissection of reactive astrogliosis and glial scar formation. Trends Neurosci. 32, 638–647.
56. White, R.E., Yin, F.Q., and Jakeman, L.B. (2008). TGF-alpha increases astrocyte invasion and promotes axonal growth into the lesion following spinal cord injury in mice. Exp. Neurol. 214, 10–24.
57. Shields, L.B., Zhang, Y.P., Burke, D.A., Gray, R., and Shields, C.B. (2008). Benefit of chondroitinase ABC on sensory axon regeneration in a laceration model of spinal cord injury in the rat. Surg. Neurol. 69, 568–577.

58. Karimi-Abdolrezaee, S., Eftekharpour, E., Wang, J., Schut, D., and Fehlings, M.G. (2010). Synergistic effects of transplanted adult neural stem/progenitor cells, chondroitinase, and growth factors promote functional repair and plasticity of the chronically injured spinal cord. J. Neurosci. 30, 1657–1676.
59. Chau, C.H., Shum, D.K., Li, H., Pei, J., Lui, Y.Y., Wirthlin, L., Chan, Y.S., and Xu, X.M. (2004). Chondroitinase ABC enhances axonal regrowth through Schwann cell-seeded guidance channels after spinal cord injury. FASEB J. 18, 194–196.
60. Karimi-Abdolrezaee, S., Schut, D., Wang, J., and Fehlings, M.G. (2012). Chondroitinase and growth factors enhance activation and oligodendrocyte differentiation of endogenous neural precursor cells after spinal cord injury. PLoS One 7, e37589.
61. Costa, S., Planchenault, T., Charriere-Bertrand, C., Mouchel, Y., Fages, C., Juliano, S., Lefrançois, T., Barlovatz-Meimon, G., and Tardy, M. (2002). Astroglial permissivity for neuritic outgrowth in neuron-astrocyte cocultures depends on regulation of laminin bioavailability. Glia 37, 105–113.
62. Frisen, J., Haegerstrand, A., Risling, M., Fried, K., Johansson, C.B., Hammarberg, H., Elde, R., Hokfelt, T., and Cullheim, S. (1995). Spinal axons in central nervous system scar tissue are closely related to laminin-immunoreactive astrocytes. Neuroscience 65, 293–304.
63. Tom, V.J., Doller, C.M., Malouf, A.T., and Silver, J. (2004). Astrocyte-associated fibronectin is critical for axonal regeneration in adult white matter. J. Neurosci. 24, 9282–9290.
64. Szabó, A., and Kálmán, M. (2004). Disappearance of the post-lesional laminin immunopositivity of brain vessels is parallel with the formation of gliovascular junctions and common basal lamina. A double-labelling immunohistochemical study. Neuropathol. Appl. Neurobiol. 30, 169–177.
65. Bush, T.G., Puvanachandra, N., Horner, C.H., Polito, A., Ostenfeld, T., Svendsen, C.N., Mucke, L., Johnson, M.H., and Sofroniew, M.V. (1999). Leukocyte infiltration, neuronal degeneration, and neurite outgrowth after ablation of scar-forming, reactive astrocytes in adult transgenic mice. Neuron 23, 297–308.
66. David, S., Bouchard, C., Tsatas, O., and Giftochristos, N. (1990). Macrophages can modify the nonpermissive nature of the adult mammalian central nervous system. Neuron 5, 463–469.
67. Faulkner, J.R., Herrmann, J.E., Woo, M.J., Tansey, K.E., Doan, N.B., and Sofroniew, M.V. (2004). Reactive astrocytes protect tissue and preserve function after spinal cord injury. J. Neurosci. 24, 2143–2155.
68. Sofroniew, M.V. (2005). Reactive astrocytes in neural repair and protection. Neuroscientist 11, 400–407.
69. Powell, E.M., Meiners, S., DiProspero, N.A., and Geller, H.M. (1997). Mechanisms of astrocyte-directed neurite guidance. Cell Tissue Res. 290, 385–393.
70. Bradbury, E.J., and Carter, L.M. (2011). Manipulating the glial scar: chondroitinase ABC as a therapy for spinal cord injury. Brain Res. Bull. 84, 306–316.
71. Busch, S.A., Horn, K.P., Cuascut, F.X., Hawthorne, A.L., Bai, L., Miller, R.H., and Silver, J. (2010). Adult NG2+ cells are permissive to neurite outgrowth and stabilize sensory axons during macrophage-induced axonal dieback after spinal cord injury. J. Neurosci. 30, 255–265.
72. Metheny-Barlow, L.J., and Li, L.Y. (2003). The enigmatic role of angiopoietin-1 in tumor angiogenesis. Cell Res. 13, 309–317.
73. Giannini, C., and Dyck, P.J. (1994). Ultrastructural morphometric abnormalities of sural nerve endoneurial microvessels in diabetes mellitus. Ann. Neurol. 36, 408–415.
74. Kalaria, R.N., and Pax, A.B. (1995). Increased collagen content of cerebral microvessels in Alzheimer's disease. Brain Res. 705, 349–352.
75. Burg, M.A., Tillet, E., Timpl, R., and Stallcup, W.B. (1996). Binding of the NG2 proteoglycan to type VI collagen and other extracellular matrix molecules. J. Biol. Chem. 271, 26110–26116.
76. Davis, G.E., Klier, F.G., Engvall, E., Cornbrooks, C., Varon, S., and Manthorpe, M. (1987). Association of laminin with heparan and chondroitin sulfate-bearing proteoglycans in neurite-promoting factor complexes from rat schwannoma cells. Neurochem. Res. 12, 909–921.
77. Muir, D., Engvall, E., Varon, S., and Manthorpe, M. (1989). Schwannoma cell-derived inhibitor of the neurite-promoting activity of laminin. J. Cell Biol. 109, 2353–2362.
78. Zuo, J., Neubauer, D., Dyess, K., Ferguson, T.A., and Muir, D. (1998). Degradation of chondroitin sulfate proteoglycan enhances the neurite-promoting potential of spinal cord tissue. Exp. Neurol. 154, 654–662.
79. Xia, Y., Zhao, T., Li, J., Li, L., Hu, R., Hu, S., Feng, H., and Lin, J. (2008). Antisense vimentin cDNA combined with chondroitinase ABC reduces glial scar and cystic cavity formation following spinal cord injury in rats. Biochem. Biophys. Res. Commun. 377, 562–566.
80. Ng, M.T., Stammers, A.T., and Kwon, B.K. (2011). Vascular disruption and the role of angiogenic proteins after spinal cord injury. Transl. Stroke Res. 2, 474–491.
81. Cardoso, F.L., Brites, D., and Brito, M.A. (2010). Looking at the blood-brain barrier: molecular anatomy and possible investigation approaches. Brain Res. Rev. 64, 328–363.
82. Huber, J.D., Egleton, R.D., and Davis, T.P. (2001). Molecular physiology and pathophysiology of tight junctions in the blood-brain barrier. Trends Neurosci. 24, 719–725.
83. Abbruscato, T.J., Lopez, S.P., Mark, K.S., Hawkins, B.T., and Davis, T.P. (2002). Nicotine and cotinine modulate cerebral microvascular permeability and protein expression of ZO-1 through nicotinic acetylcholine receptors expressed on brain endothelial cells. J. Pharm. Sci. 91, 2525–2538.
84. Fischer, S., Wobben, M., Marti, H.H., Renz, D., and Schaper, W. (2002). Hypoxia-induced hyperpermeability in brain microvessel endothelial cells involves VEGF-mediated changes in the expression of zonula occludens-1. Microvasc. Res. 63, 70–80.
85. Mark, K.S., and Davis, T.P. (2002). Cerebral microvascular changes in permeability and tight junctions induced by hypoxia-reoxygenation. Am. J. Physiol. Hearp Circ. Physiol. 282, H1485–H1494.
86. Bukhari, N., Torres, L., Robinson, J.K., and Tsirka, S.E. (2011). Axonal regrowth after spinal cord injury via chondroitinase and the tissue plasminogen activator (tPA)/plasmin system. J. Neurosci. 31, 14931–14943.
87. Cholas, R., Hsu, H.P., and Spector, M. (2012). Collagen scaffolds incorporating select therapeutic agents to facilitate a reparative response in a standardized hemiresection defect in the rat spinal cord. Tissue Eng. Part A 18, 2158–2172.
88. Wang, X., Hasan, O., Arzeno, A., Benowitz, L.I., Cafferty, W.B., and Strittmatter, S.M. (2012). Axonal regeneration induced by blockade of glial inhibitors coupled with activation of intrinsic neuronal growth pathways. Exp. Neurol. 237, 55–69.

Address correspondence to:
Sylvia Soares, PhD
UPMC Univ Paris 06
UMCR18-Neuroscience Paris Seine-IBPS
CNRS UMR8246
7 Quai St Bernard
75005 Paris
France

E-mail: sylvia.soares@snv.jussieu.fr